NANO LETTERS
Cite This: Nano Lett. XXXX, XXX, XXX−XXX
Letter
pubs.acs.org/NanoLett

Exciton-Delocalizing Ligands Can Speed Up Energy Migration in Nanocrystal Solids

Michael S. Azzaro,[†] Amro Dodin,[§] Diana Y. Zhang,[‡] Adam P. Willard,[§] and Sean T. Roberts*[,†]

[†]Department of Chemistry and [‡]McKetta Department of Chemical Engineering, The University of Texas, Austin, Texas 78712, United States

[§]Department of Chemistry, Massachusetts Institute of Technology, Cambridge, Massachusetts 02139, United States

Supporting Information

ABSTRACT: Researchers have long sought to use surface ligands to enhance energy migration in nanocrystal solids by decreasing the physical separation between nanocrystals and strengthening their electronic coupling. Exciton-delocalizing ligands, which possess frontier molecular orbitals that strongly mix with nanocrystal band-edge states, are well-suited for this role because they can facilitate carrier-wave function extension beyond the nanocrystal core, reducing barriers for energy transfer. This report details the use of the exciton-delocalizing ligand phenyldithiocarbamate (PDTC) to tune the transport rate and diffusion length of excitons in CdSe nanocrystal solids. A film composed of oleate-terminated CdSe nanocrystals is subjected to a solid-state ligand exchange to replace oleate with PDTC. Exciton migration in the films is subsequently investigated by femtosecond transient absorption. Our experiments indicate that the treatment of nanocrystal films with PDTC leads to rapid (∼400 fs) downhill energy migration (∼80 meV), while no such migration occurs in oleate-capped films. Kinetic Monte Carlo simulations allow us to extract both rates and length scales for exciton diffusion in PDTC-treated films. These simulations reproduce dynamics observed in transient absorption measurements over a range of temperatures and confirm excitons hop via a Miller−Abrahams mechanism. Importantly, our experiments and simulations show PDTC treatment increases the exciton hopping rate to 200 fs, an improvement of 5 orders of magnitude relative to oleate-capped films. This exciton hopping rate stands as one of the fastest determined for CdSe solids. The facile, room-temperature processing and improved transport properties offered by the solid-state exchange of exciton-delocalizing ligands show they offer promise for the construction of strongly coupled nanocrystal arrays.

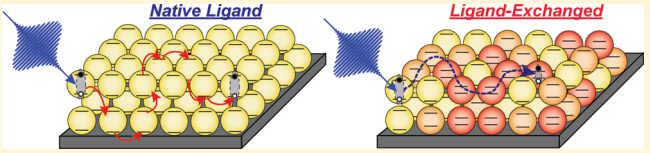

KEYWORDS: *quantum dot solid, kinetic Monte Carlo, ligand exchange, phenyldithiocarbamate, exciton transport, transient absorption, electronic coupling*

Semiconductor nanocrystals (NCs) have long been candidates for low-cost, solution-processable optoelectronics. Despite this promise, they have yet to find industrial-scale integration into many applications.[1−3] Barriers to their incorporation in electronics result, in part, from the low carrier mobility and poor conductivity of native ligand-capped NC films. The long, carbon-chain ligands (typically 12−30 carbons) employed during NC synthesis hinder energy transport by forming an insulating shell around each NC that excitons must traverse to diffuse within a film.[4−7] Researchers have sought to improve energy transport by exchanging these ligands for shorter ones that decrease interparticle separation and reduce the effective gap excitons must tunnel through to move from one NC to another.[8−13] At present, the fastest reported rates for energy transfer in NC solids fall in the range of tens to hundreds of picoseconds per hop between NCs.[14−17] Typically, these rates have been obtained by exchanging long, insulating native ligands for shorter ones.

More recently, a strategy that builds upon this approach has emerged wherein insulating ligands are replaced with so-called exciton-delocalizing ligands (EDLs), molecules with frontier molecular orbitals that can efficiently hybridize with NC band-edge states.[18−23] As such, EDLs can form hybrid states in which carrier density extends from the NC surface into their ligand shell. Such states reduce not only the size of the tunneling barrier between NCs but also its height by altering NC electronic structure. When properly designed, EDLs may be able to enhance electronic coupling between NCs, such that its strength becomes on par with the energetic disorder between neighboring NCs that give rise to Anderson localization.[24,25] In such a scenario, carrier transport in NC solids can proceed through a series of "mini bands",[26] strongly coupled regions of a film wherein carrier transport unfolds coherently over short distances.[26−29] Such films can display improved transport properties while maintaining desirable size-tunable properties imparted by quantum confinement.[20,30,31]

One class of EDLs with the potential to enhance carrier transport in NC films are dithiocarbamates.[32−38] In particular, phenyldithiocarbamate (PDTC) possesses a highest occupied molecular orbital energy and symmetry that allow it to strongly couple with states within the valence band of CdSe NCs.[39]

Received: March 17, 2018
Published: April 13, 2018

DOI: 10.1021/acs.nanolett.8b01079
Nano Lett. XXXX, XXX, XXX−XXX

Functionalizing CdSe NCs with PDTC allows hole-carrier density to extend into the PDTC ligand shell, which reduces their exciton confinement energy.[32] This is evidenced through a red shift of NC absorption spectra upon PDTC functionalization. In solution, PDTC facilitates hole transfer to surface-bound ligands on sub-picosecond time scales,[35,36,38] suggesting PDTC substitution could similarly be used to enhance energy transfer between NCs in solid films. For this reason, we have examined CdSe NC films exchanged with PDTC ligands to determine the extent to which EDLs can enhance exciton transport in NC films.

Measuring transport in NC films presents a number of practical challenges as electrical measurements require NCs be integrated into device geometries such as field-effect transistors and photovoltaic cells.[20,26,40,41] In such devices, the nature of the electrical contacts formed to a NC film can strongly impact device performance[42−44] and, consequently, the derived values for exciton diffusion rates and carrier mobilities. To circumvent this problem, researchers have devised ways to extract the diffusion lengths and hopping rates of carriers in films using optical methods as a proxy for electrical device measurements.[14,45−50] A recent study by Gilmore et. al has shown time-resolved spectroscopic measurements coupled with simulations can be used to extract energy transport parameters for ligand-exchanged PbS NC solids.[14] In particular, transient absorption spectroscopy (TA) was used to track time-dependent changes in the average energy of the band-edge exciton of excited PbS NCs by monitoring the spectral position of photobleaching bands. Using a kinetic Monte Carlo simulation to fit the transient data, they were able to follow charge transport in homogeneously broadened NC solids and extract carrier-hopping rates and mobility values.

In this manuscript, we have used a similar approach to track exciton migration in PDTC-treated CdSe films and assess the impact of this EDL on exciton diffusivity. TA measurements performed on PDTC-exchanged films display a rapid, sub-picosecond decrease of the average energy of excited carriers within a NC film. These dynamics are not observed in oleate-capped NC films, suggesting PDTC treatment reduces barriers hindering exciton transport within NC solids. To quantitatively extract a hopping rate between NCs, we have developed a site-based kinetic Monte Carlo model that properly accounts for the size dispersion of our NC films as well as changes in NC exciton energies and hopping rate upon treatment with PDTC. To properly account for time-dependent changes observed in TA measurements performed as a function of temperature, we find that we need to employ a Miller−Abrahams model[51] to describe exciton hopping. This indicates exciton transfer occurs not by Förster resonance energy transfer but rather via carrier tunneling. Trajectories computed with this model reveal hops between NCs occur as fast as 200 fs in PDTC-exchanged films, whereas excitons produced in oleate-capped films display hopping rates that are 5 orders of magnitude slower. Interestingly, our experimental data indicates PDTC treatment also speeds up carrier recombination, which unfolds over hundreds of picoseconds. The incorporation of a relaxation rate in our kinetic Monte Carlo simulations that scales with the number of PDTC molecules coordinated to CdSe NCs reproduces this result. This finding is in qualitative agreement with prior work that demonstrated PDTC can enhance the radiative recombination of excitons in CdSe NCs.[34,52] Importantly, the hopping rates measured as a result of PDTC exchange fall among the fastest reported for NC solids. This suggests that treating NC surfaces with EDLs can form an effective strategy for speeding up energy transport.

Results and Discussion. The CdSe NC films used in this study were produced via a facile, room-temperature spin-coating procedure that yields highly uniform and optically transparent thin films (~220 nm thickness) on SiO_2 substrates. The details of this procedure can be found in the methods section below. The ability of this spin-casting process to produce NC films with long-range order was confirmed via scanning electron microscopy (SEM), which showed films display uniform topography over tens of microns (Figure 1, top). After we prepared oleate-capped NC films, a solid-state PDTC ligand exchange was carried out that alters both the packing of the film and its electronic structure. Profilometry measurements revealed that PDTC ligand exchange results in a decrease of the film's height to 90 nm, a 59% reduction in film thickness (Figure S1). Assuming no NC loss during ligand

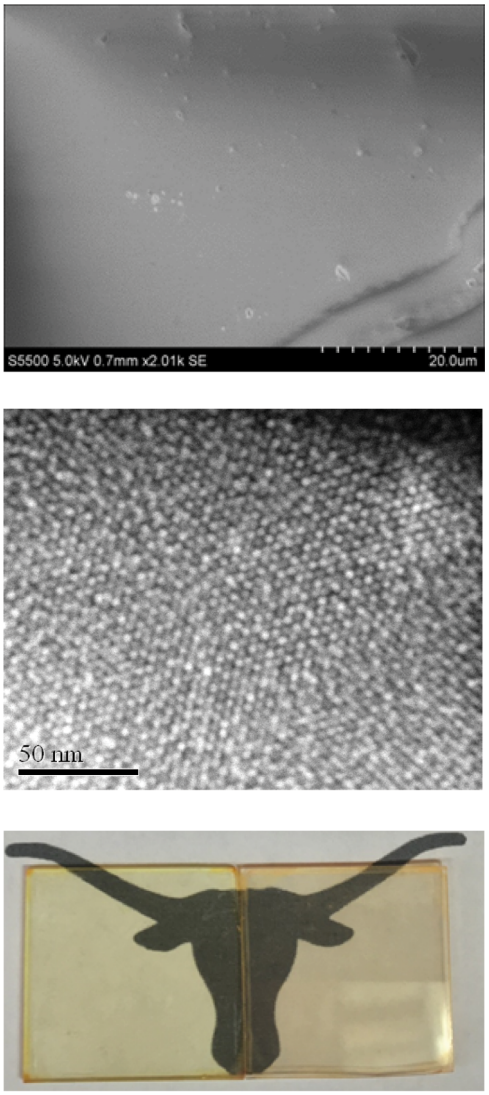

Figure 1. (Top) SEM image of CdSe−oleate film showing the long-range order and film homogeneity. (Middle) Scanning transmission electron microscopy image showing oleate-capped NC packing structure. (Bottom) Photograph highlighting the optical clarity of CdSe−oleate (left) and CdSe−PDTC (right) films. Note the color change of the film after ligand exchange.

DOI: 10.1021/acs.nanolett.8b01079
Nano Lett. XXXX, XXX, XXX−XXX

exchange, this procedure yields a film with an average center-to-center separation of 3.7 ± 0.5 nm. We note this degree of compression is consistent with the difference in the end-to-end length between PDTC (0.7 nm) and oleate ligands (2 nm) estimated from geometry optimized DFT calculations using a B3LYP functional and 6-311+G** basis set. Assuming NC films can be described as a collection of closely-packed spheres with diameters given by the NC diameter plus a single ligand, we predict the film should decrease in volume by ∼65% upon full PDTC exchange if the ligands were perfectly interdigitated. This change is supported by transmission electron microscopy (TEM) measurements (Figure 1, middle) that show following ligand exchange the NC center-to-center distance decreases from 4.7 ± 0.5 to 4.1 ± 0.7 nm (Figure S2). While our results below suggest that different NCs within the film bind varying amounts of PDTC following solid-state ligand exchange, these calculations imply that the amount of oleate that remains in the film is somewhat small.

,In addition to structural changes, ligand exchange with PDTC also modifies the optical properties of CdSe films. Figure 2 compares the optical spectra of CdSe films composed of 2.3 nm NCs both before and after ligand exchange to replace oleate with PDTC. Upon PDTC treatment, the lowest-energy exciton band (X1) of a CdSe film undergoes a red shift of ∼70 meV. A similar shift of the emission line shape of the film is also seen, as is the broadening of both the absorption and the emission bands of the ligand-exchanged NC solid. While the red shift has been previously attributed to a relaxation of confinement at the NC−ligand interface due to mixing between the electronic states of the NC and PDTC ligand,[32,3652] broadening of the X1 band and emission line width upon PDTC exchange have not previously been reported.

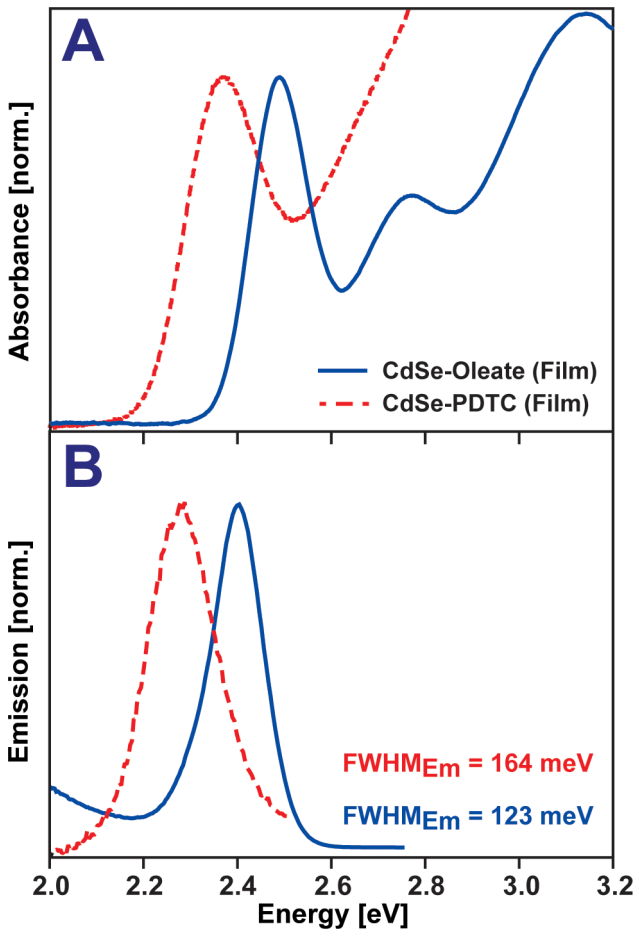

Figure 2. (A) Absorption spectra of CdSe−oleate (blue line) and CdSe−PDTC (dashed red line) films. (B) Emission spectra of CdSe−oleate (blue line) and CdSe−PDTC (dashed red line) films. The full width at half-maximum values for the band-edge emission of each film are reported.

A pair of different effects could give rise to this observed broadening. First, the ability of PDTC to allow carriers to partially extend into the CdSe ligand shell could enhance electronic coupling between neighboring NCs, leading to a modification of their spectra. Prior work on NC superlattice films and ligand-exchanged solids provides some precedence for this scenario. In particular, PbSe superlattices display similar broadening of their optical spectra that has been attributed to necking between particles within the lattice.[53] Likewise, CdSe films subjected to a solid-state ligand exchange process in which native ligands were exchanged for *tert*-butylthiol ligands and subsequently annealed display similarly broadened spectra that were assigned to an increase in connectivity between NCs within the film.[54] Alternatively, as the magnitude of the change in the X1 exciton energy depends on the number of PDTC molecules that coordinate to a NC's surface,[55] heterogeneity of PDTC exchange within the film could produce a distribution of exciton energies that would similarly give rise to a red-shifted but broadened X1 absorption band. In this latter case, exciting the ensemble of NCs that make up a film could lead to a net migration of energy from high-energy to lower-energy sites over time if the exciton transfer rate is fast relative to the exciton lifetime.

To test these hypotheses, we used transient absorption (TA) measurements to follow exciton relaxation dynamics of PDTC-exchanged films following photoexcitation. In the TA experiment, a femtosecond pump pulse excites an ensemble of NCs whose ensuing dynamics are read out by a time-delayed, broadband white-light probe pulse. As the pump pulse removes carriers from the valence band and places them into the conduction band, this lowers the absorptivity of the X1 state, creating a transient photobleach of this transition, commonly referred to as the "B1 bleach" in NC studies.[56,57] The peak position of this band reflects the average energy of excited NCs within a film.[14] Changes in the center position of this peak can thus signal energy migration between neighboring NCs.

Figure 3A plots TA spectra of a PDTC-exchanged film following photoexcitation at 400 nm (3.1 eV). Examining the data at a pump−probe delay of 200 fs, a decrease in absorption attributed to the B1 band is observed whose maximum falls at 2.32 eV, an energy close to the peak absorptivity of the X1 state in the film's steady-state absorption spectrum (Figure 2B). As the pump−probe delay is increased, the B1 band undergoes a rapid red shift, lowering its peak energy to ∼2.24 eV over the course of 1 ps. We note TA experiments performed on PDTC-exchanged NCs in solution do not show this shifting behavior (Figure S3), indicating it is not due to carrier cooling within individual NCs but rather must result from interactions between NCs within the film. Given our prior hypotheses for the observed broadening of the steady-state absorption spectra of PDTC-exchanged films, we note a shift of the B1 band to lower energy over time is consistent with excitations moving within PDTC-exchanged films along an energetic gradient toward lower-energy NCs with a high degree of PDTC substitution.

DOI: 10.1021/acs.nanolett.8b01079
Nano Lett. XXXX, XXX, XXX−XXX

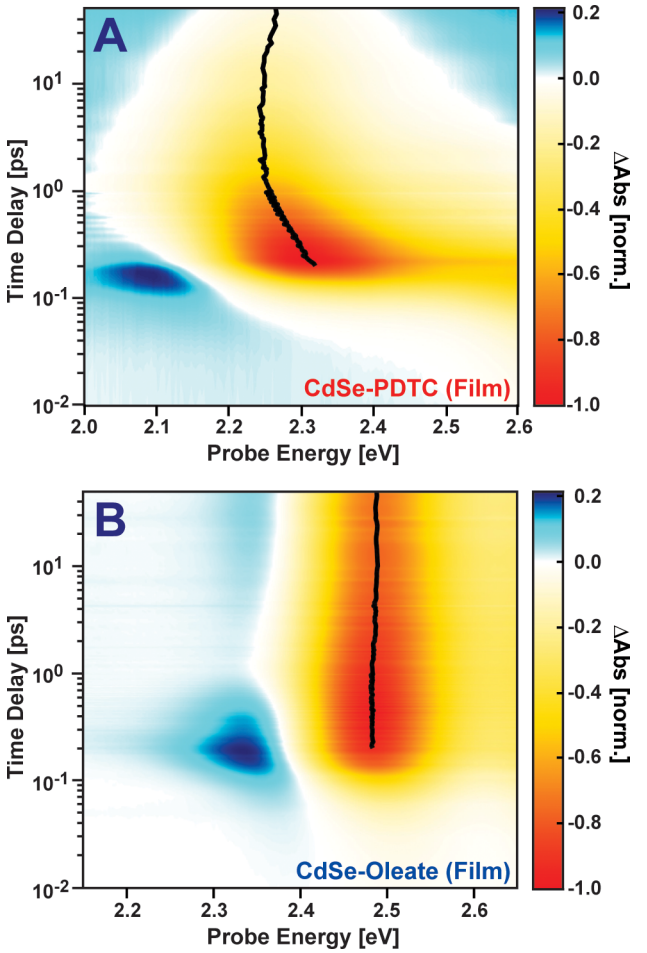

Figure 3. TA spectra of (A) CdSe–PDTC films and (B) CdSe–oleate films that highlight time-dependent changes in the position of the NC B1 band within the first 50 ps following excitation. Signal amplitudes shown in red and orange correspond to absorption decreases (photobleaching), while signals shown in blue denote absorption gains. Black lines indicate the energy of the B1 bleach maximum as a function of time.

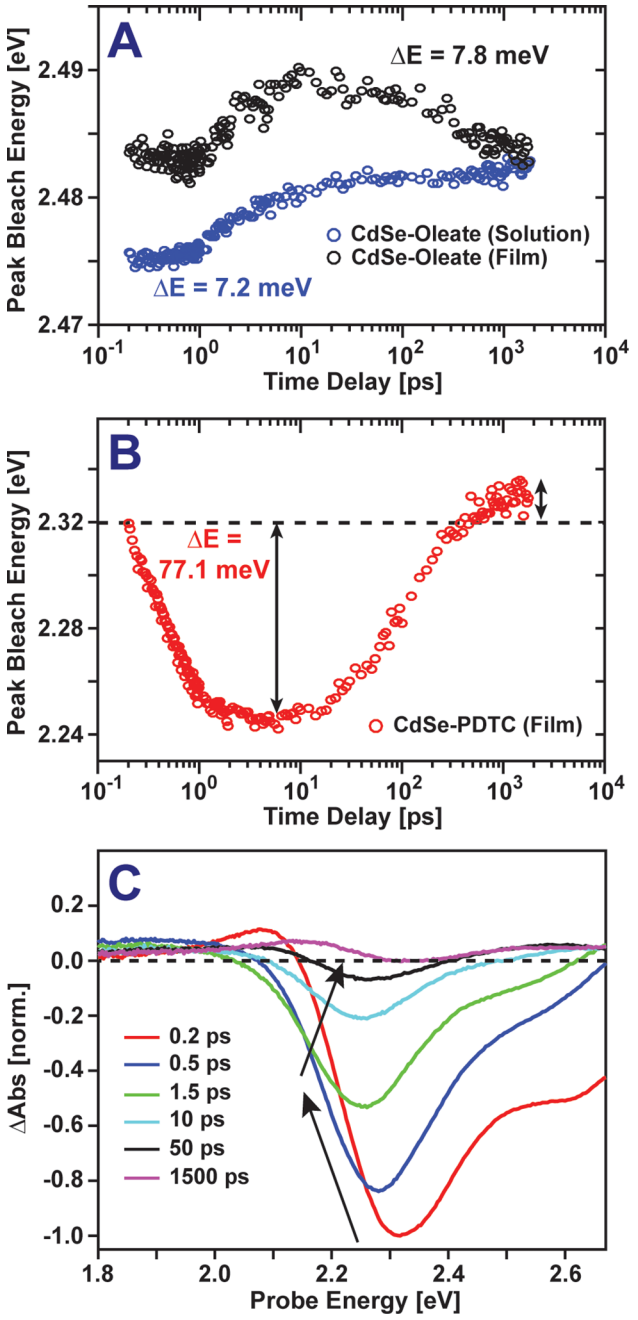

Figure 4. (A) Center-peak B1 bleach energy of a CdSe–oleate solution (blue circles) and film (black circles) as a function of pump–probe time delay. (B) Center-peak B1 bleach energy of a CdSe–PDTC film as a function of pump–probe time-delay. (C) TA spectrum of CdSe–PDTC film highlighting B1 bleach evolution (black arrows) over the lifetime of the experiment.

We compare this result to similar TA measurements conducted on films composed of NCs capped with native oleate ligands (Figure 3B). We observe no appreciable red shift of the B1 band within the first 50 ps following photoexcitation. Rather, upon plotting the center position of the B1 band (Figure 4A, black), we see an ~8 meV increase in the energy of this feature over 10 ps. As isolated CdSe NCs in solution display a similar increase in the energy of the B1 band upon excitation (Figure 4A, blue), this shift cannot be tied to energy migration within the native ligand-capped NC film. While we have focused our discussion on the photobleaching contributions to the B1 band, a portion of this feature's amplitude on its lower energy side arises from stimulated emission from X1 excitons. A loss of stimulated emission can shift the B1 band to higher energy. Such a stimulated emission loss can result from the trapping of photoexcited holes, which has been shown to occur rapidly in CdSe NCs.[36,58]

Following its shift to higher energy, the peak of the B1 band of CdSe–oleate films returns to its starting position over hundreds of picoseconds. This shift back toward lower energy is absent from the TA spectra of individual, oleate-capped NCs in solution. While the synthetic methodology we used to produce CdSe NCs was selected due to its ability to produce NCs with a narrow size distribution, the emission line width measured for the oleate-capped NC film is 123 meV, which is ~10–20 meV larger than the predicted homogeneous line width for uniform CdSe NCs with an exciton energy of 2.48 eV.[59,60] Thus, the ~8 meV red shift we observe for the oleate-capped NC film likely results from energy migration within the film toward larger NCs with lower X1 energies. However, the time scale observed for this migration, 353 ps, is nearly 3 orders of magnitude slower than that found in PDTC-functionalized

DOI: 10.1021/acs.nanolett.8b01079
Nano Lett. XXXX, XXX, XXX–XXX

films, ~400 fs (Figure S3), indicating functionalization of NCs with PDTC significantly speeds energy transport.

Shifting our focus back to dynamics within PDTC-functionalized films, we find that over a few hundred picoseconds, the peak of the B1 bleach increases in energy and ultimately settles on a value that is 8.6 meV higher in energy than its initial position (Figure 4B). This increase in the B1 band center position is unexpected as exciton migration within a film should only cause this band to decrease in energy rather than increase. As such, a different fundamental process must underlie the observed dynamics. Examining our TA spectra further, we note the increase in the B1 band center position is correlated with a loss of its amplitude (Figure 4C), suggesting that exciton relaxation is responsible for the observed spectral shifting dynamics. Both experiments[34,36] and theory[52] have shown PDTC can increase an NC's radiative rate by enhancing the density of states at the NC band edge. Likewise, PDTC ligand exchange can induce some degree of NC surface reconstruction that accelerates nonradiative carrier recombination when improperly passivated.[34,36] Therefore, excitons in NCs with a high degree of PDTC substitution should decay more rapidly compared to excitons in NCs with fewer PDTC molecules bound to their surface. We hypothesize this effect is responsible for the long-time B1 shifting dynamics shown in Figure 4B. As more highly PDTC substituted sites should decay preferentially, the longtime behavior is dominated by those less-substituted, higher-energy sites that have slower decay rates. This is reflected in the TA spectrum as a blueshift of the B1 bleach maximum at long time delays. Thus, we interpret the observed shifting of the B1 band of PDTC-functionalized films as arising from two distinct phenomena: (1) rapid exciton migration to low-energy, highly PDTC-substituted NC sites on a subpicosecond time scale, and (2) the accelerated decay of excitons at these low-energy sites.

While extracting time scales and the magnitude of the downhill energy migration from TA spectra provides some measure of PDTC's impact on the transport properties of NC films, to build a comprehensive picture of the effects of PDTC exchange, we have turned to simulations to provide a deeper physical understanding of this process. To extract relevant transport parameters, such as the carrier diffusion length, transport rate, and mechanism, we have developed a kinetic Monte Carlo (KMC) model that can accurately reproduce the changes we observe in TA spectra of NC films. In this model, the CdSe film is described as an ordered array of 16 000 NCs arranged at the vertices of a three-dimensional face-centered cubic (FCC) lattice composed of 40 close-packed 20 × 20 layers and periodically replicated in the x and y dimensions. The inter-NC spacing is determined by the FCC lattice constant, which we set based on experimental measurements. To account for energetic variations within the NC population, we assigned each NC in the model an intrinsic energy, $E_i^{(0)}$, assigned randomly from a Gaussian distribution, which is parametrized based on experimental emission spectra.

We model the effect of PDTC substitution by assuming each PDTC ligand produces a redshift in the NC energy of α = −3.46 meV. The value of α is obtained from the linear absorption spectra of colloidal oleate-capped and PDTC-exchanged NCs and is consistent with previously reported values for colloidal CdS NCs.[55] We also assume each PDTC ligand increases the excited-state decay rate by an amount of κ_D = 1.22 ns^{-1}, which is obtained by fitting the TA spectra of colloidal PDTC-exchanged NCs (section SVIII of the Supporting Information). In this way, if NC i has n_i substituted PDTC ligands, it will have an energy of $E_i = E_i^{(0)} + n_i\alpha$ and an excitation decay rate of $k_D = k_D^{(0)} + n_i\kappa_D$, where $k_D^{(0)}$ is the decay rate of an unsubstituted site. We assign the PDTC substitution number, n_i, randomly based on a Poisson distribution with a mean of 24 substituted ligands, consistent with Fourier transform infrared (FTIR) measurements of oleate loss in the exchange process[36] and taking into account that each PDTC molecule displaces two oleate ligands.[55]

To describe exciton transport in NC films, a model is required that predicts how the rate of exciton transfer between NCs varies with the energy difference between NC sites and their spatial separation. In weakly coupled NC arrays, Förster resonance energy transfer (FRET) has been suggested to be the dominant mechanism of energy transfer.[16] However, a calculation of the FRET rate between two CdSe NCs separated by a single PDTC molecule predicts a hopping rate of several nanoseconds, which is orders of magnitude slower than the shifting behavior we observe for the B1 band experimentally. For this reason, we have chosen to instead model exciton transport in NC films via a carrier tunneling mechanism. Motivated by the exponential distance dependence of carrier tunneling rates, we assume transport is dominated by incoherent next-neighbor hops from site i to site j with a Miller−Abrahams rate:[51]

$$k_{i\to j} = \begin{cases} k_T \exp\left(-\dfrac{(E_j - E_i)}{2k_B T}\right), & \text{if } E_j > E_i \\ k_T, & \text{otherwise} \end{cases} \quad (1)$$

where E_n is the energy of site n, k_T is a characteristic transport rate, and $(E_j - E_i)/2$ is the energy difference between an exciton on particle j and on particle i under the effective mass approximation. Direct hops between particles that do not neighbor one another are neglected in our model because a similar KMC study of NC films found no improvement in model performance by including coupling beyond nearest-neighbor sites.[14]

The initial excitation seen in the TA spectrum of the PDTC exchanged film is significantly blue-shifted from the film's emission spectrum, indicating a nonequilibrium population of sites is prepared by the pump pulse. We therefore model the initial population of excitations by randomly selecting NCs with a bias on the intrinsic NC energy, $E_i^{(0)}$, designed to reproduce the initial TA bleach peak. Once initialized, we simulate the dynamics of individual noninteracting excitons using a KMC algorithm. For this algorithm, at each KMC step the exciton can either hop to a NC on a neighboring lattice site, with rate $k_{i\to j}$, as expressed in eq 1, or can decay to the ground state (thereby terminating the trajectory) with rate k_D. The transport rates can then be fit to the initial red-shift behavior giving a transport rate of 6.7 × 10^{-5} ps^{-1} for the oleate-capped films and 4.6 ps^{-1} for the PDTC-exchanged film, indicating an increase in the transport rate by nearly 5 orders of magnitude (Figure 5). Correspondingly, an excitation in the PDTC exchanged film travels ~10−12 lattice units in its ~100 ps lifetime, while an exciton in the oleate capped film travels ~4 lattice units in its ~1 ns lifetime. We conclude that the rapid red shift seen in PDTC-treated films results from a significant enhancement of the exciton hopping rate, which our KMC simulations suggest falls on the order of 200 fs per hop. Thus, PDTC treatment appears to enhance carrier tunneling in NC films.

DOI: 10.1021/acs.nanolett.8b01079
Nano Lett. XXXX, XXX, XXX−XXX

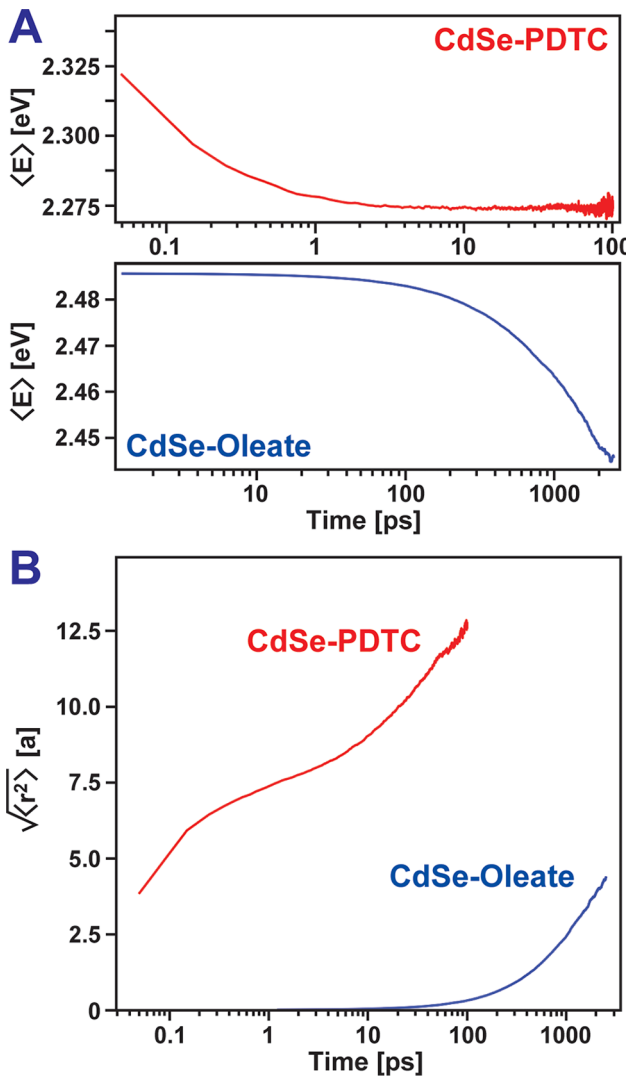

Figure 5. Time series of the (A) mean exciton energy and (B) root mean squared displacement for PDTC-exchanged (red line) and oleate-capped (blue line) NC films extracted from KMC simulations. The mean exciton energy corresponds to the bleach peak position of the TA spectra, while the root mean squared displacement is reported in units of the lattice constant, *a*. Note the difference in axis scales for the PDTC-exchanged and oleate-capped NC films in panel A.

Earlier, we hypothesized the blue shift we observe experimentally on longer time scales results from the rapid decay of excitations at highly substituted PDTC sites. Consistent with this hypothesis, when we constrain our KMC model using experimental parameters, we find a majority of excitations decay before reaching time delays at which we experimentally find the average excitation energy to shift back to higher energy. Thus, it is a very small fraction of exceptionally long-lived excitons that are responsible for the eventual return of the CdSe−PDTC film B1 bleach to high energy. Capturing this effect in simulation necessitates the generation of a very large ensemble of exciton trajectories, of which only a few ultimately contribute to the long-time blue shift. As such, accurately reproducing this behavior requires the use of long simulation times and averaging over multiple realizations of the energetic disorder in our system. To determine if our KMC model can produce a blue shift of the B1 bleach, we have explored how the behavior of trajectories change when the decay rate asymmetry, κ_D, is varied. Increasing this parameter will accelerate the rate at which low-energy excitations decay and thereby allow shorter trajectories to be used to determine if the model predicts a bleach blue shift. Indeed, we find as this value is increased the model exhibits a range of different behaviors, some of which display a bleach blue shift, while others do not. This suggests that the behavior predicted by our model is sensitive to the relative rates for energy transport and excitation decay.

To explore how competition between different microscopic parameters work in concert to give rise to the observed red shift and subsequent blue shift in PDTC-treated films, we perform a sweep through these parameters. To facilitate this sweep, a few simplifying assumptions were made to reduce the dimensionality of the model's parameter space. First, all NCs were taken to have the same intrinsic energy. The energy variance is, therefore, a result of PDTC substitution only. The initial exciton ensemble is then created by a uniform sampling of all NC sites. The parameter sweep is then performed across three non-dimensional ratios of the model parameters.

The ratio $k_T/k_D^{(0)}$ measures competition between transport and exciton decay and is proportional to the number of hopping events in an unsubstituted film. Second, $\Delta k_D/k_D^{(0)}$, where $\Delta k_D = \kappa_D \bar{n}$, measures the preferential decay of more substituted sites where $\bar{n}$ is the mean substitution number. Finally, $k_B T/\Delta E$ is a normalized temperature measuring the size of thermal fluctuations relative to the standard deviation in site energies $\Delta E = \alpha \bar{n}$. Therefore, the ratio $k_T/k_D^{(0)}$ controls the thermal relaxation that gives rise to the red shift, while the ratio $\Delta k_D/k_D^{(0)}$ controls the asymmetric decay responsible for the blue shift.

Representative time series showing the evolution of the average exciton energy as a function of these parameters are shown in Figure 6, which explores how varying the relative rates of excitation transfer and decay influence the mean excitation energy of the NC ensemble. Our sweep identifies three characteristic behaviors for the photobleaching of the NC ensemble: (i) red shift only (highlighted in red), (ii) blue shift only (highlighted in blue), and (iii) red shift followed by a blue back-shift (highlighted in green). A red shift of the mean excitation energy has been observed in previous studies of ethanethiol-capped NC films[14] and can be attributed to thermalization of the exciton ensemble. This behavior is a direct consequence of the thermodynamic detailed balance condition. In contrast, a blue shift is a new behavior unique to the PDTC-exchanged film. This occurs due to the preferential decay of highly substituted low-energy sites, leading to an oversampling of higher-energy unsubstituted sites at long times and a corresponding blue shift of the mean energy. The red shift therefore occurs due to thermodynamic equilibration within the excited-state manifold, while the blue shift is a competing nonequilibrium effect.

Examining the results of our parameter sweep, we find that when there is little decay-rate asymmetry ($\Delta k_D/k_D^{(0)} \ll 1$), a red shift is seen when the thermal fluctuations are smaller than the standard deviation in site energies. Furthermore, the size of the shift is determined by the ratio k_T/k_D. This is consistent with previous studies[14] and with the thermalization mechanism for the red-shift. As the decay rate asymmetry is increased, a system that initially displayed a red shift only first shows a smaller red shift followed by a subsequent back-shift, then a linear blue shift only. This illustrates the competition between the approach to thermal equilibrium and the nonequilibrium decay-rate

DOI: 10.1021/acs.nanolett.8b01079
Nano Lett. XXXX, XXX, XXX−XXX

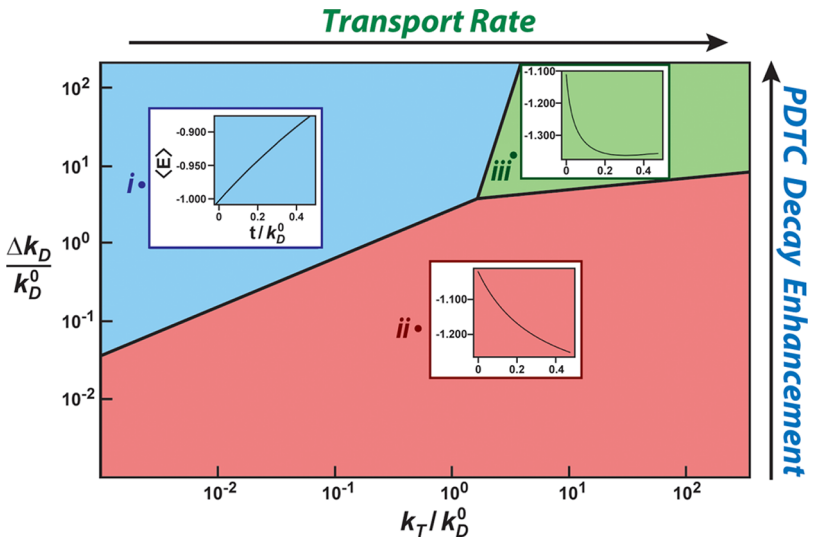

Figure 6. Parameter sweep showing how the behavior of the mean exciton energy in KMC simulations varies with changing exciton transport rate and PDTC decay enhancement. Regions in blue display only an increase in average exciton energy (i), regions in red show a decrease (ii), and those in green show a decrease followed by an increase (iii).

asymmetry and is consistent with the selective-decay mechanism for the blue-shift. We find that only over a relatively narrow range of parameters do we observe a red shift followed by a blue shift (Figure 6, region iii).

We also note our kinetic model makes some clear predictions regarding how rates for exciton transport and relaxation change with temperature. As we cool the PDTC-exchanged film, the initial rate of downhill energy migration is expected to be unchanged because this process is not thermally activated. Over time, as excitons encounter local minima, the residence time spent in these wells increases with decreasing temperature. Thus, we expect the rate at which excitons access the lowest energy sites with the highest exciton recombination rates should slow. Projecting these dynamics onto our bleach shifting behavior, as temperature is lowered, we expect to observe a negligible change in the red-shifting behavior at short time delays and a suppression of the blue-shift recovery at long delays as exciton migration to sites favoring exciton recombination is suppressed. These predictions are supported by experimental TA spectra of PDTC-exchanged films measured at 78 and 294 K (Figure 7A). These data show that the time scale associated with the initial red shift of the NC X1 photobleach displays little change with decreasing temperature, while the blue shift that occurs over hundreds of picoseconds at 294 K is completely suppressed at 78 K. Figure S8 shows that the inhibition of the blue shift of the NC X1 band at low temperatures is correlated with a lengthening of the exciton lifetime, lending further support to our model.

In Figure 7B, we use our kinetic model to make predictions regarding the behavior of excitations in PDTC-exchanged NC films over a larger temperature range than we can access experimentally. These calculations are performed for a set of parameters that, according to the parameter sweep in Figure 6, predict a red-shift followed by a blue-shift at temperatures where the energetic disorder in the system is similar to thermal energy ($k_T/k_D^{(0)} = \Delta k_D/k_D^{(0)} = 10$). At temperatures where the thermal energy is comparable to the distribution of site energies ($k_BT/\Delta E = 1$, Figure 7B, middle panel), our KMC model predicts a rapid red shift of the average exciton energy followed by a slower recovery resulting from exciton decay at highly

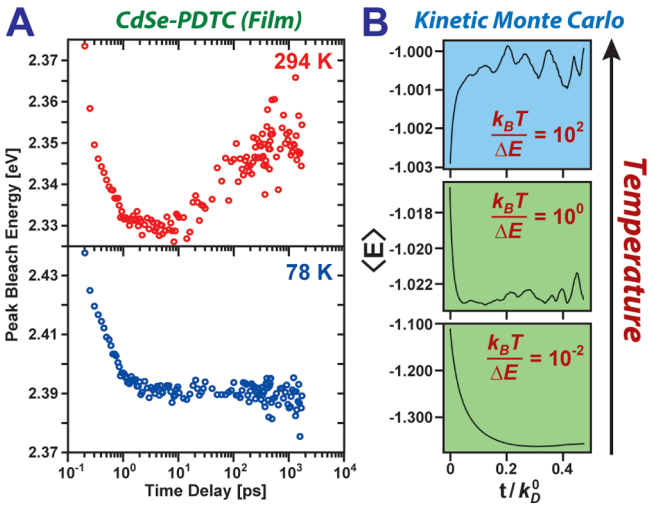

Figure 7. (A) Peak B1 bleach energy of a CdSe−PDTC film measured as a function of pump−probe time delay at 294 K (top, red circles) and 78 K (bottom, blue circles). (B) KMC parameter sweep showing the influence of temperature on exciton transport for a fixed $k_T/k_D^{(0)}$ ratio of 10 and a fixed $\Delta k_D/k_D^{(0)}$ ratio of 10.

substituted PDTC sites. This behavior is comparable to our experimental results at room temperature and, according to the scaling relationships extracted from our sweep, we conclude the experimental parameters derived from PDTC-functionalized films should give rise to a blue shift occurring on time scales on the order of 0.1−1 ns, which is consistent with our experimental data. As the temperature is lowered ($k_BT/\Delta E = 0.01$, Figure 7B, bottom panel), we find the blue shift of the average exciton energy at longer delays is suppressed, similar to our results at 78 K. The plotted data trace also shows a slowing of the initial red shift of the average exciton energy, which is not as readily apparent in our experimental data at 78 K. However, this occurs as the temperature variation shown for the model corresponds to a 100× decrease in the temperature, whereas we only explore a 4× decrease experimentally, which would impact the extent to which local trapping of excitons during downhill energy migration influences their dynamics.

DOI: 10.1021/acs.nanolett.8b01079
Nano Lett. XXXX, XXX, XXX−XXX

Experimentally, heating our films above 400 K leads to PDTC degradation (Figure S9). However, using our KMC model, we can predict how excitons move in a disordered NC lattice when the thermal energy exceeds the site disorder ($k_BT/\Delta E = 100$, Figure 7B, top panel). In this case, we find lowering the energetic penalty for occupying a high-energy site leads to the absence of a decrease of the average exciton energy at short time delays as each site in the NC lattice gains similar probability for exciton occupation. Over time, we observe an increase in the average exciton energy that stems from preferential relaxation at low-energy sites. The overall magnitude of this shift, however, decreases with increasing temperature as the thermal energy simply outweighs the distribution of site energies, preventing exciton pooling at low-energy sites.

The model we have employed is similar to one we previously used to describe exciton migration in NC superlattices.[14] However, we wish to point out this current model includes a significant feature that is unique to this work. Specifically, this model includes a source of disorder corresponding directly to variations in PDTC coverage. Unlike the standard inhomogeneous disorder, this PDTC-based disorder affects exciton decay rate. This has two important effects: (1) this disorder leads to spatially heterogeneous decay rates, and (2) this disorder couples exciton energy and decay rate, directly correlating these two properties. We find that this drastically alters the nonequilibrium exciton statistics because the interaction between transport and spatially heterogeneous decay leads to unexpected behavior. Here, this correlation is responsible for the novel nonmonotonic behavior observed in the nonequilibrium energy of the NC exciton ensemble, while in another study, correlation between excitation energy and decay rate has been found to enhance near-infrared emission from PbS NCs interfaced with J-aggregate assemblies.[61] Our results suggest there exists potential to harness correlated transport and decay in the design of nanostructured materials.

Examining the exciton hopping time scale extracted from our KMC model for PDTC-functionalized films, 200 fs, we find it is very fast compared to values reported by other groups. For example, energy-hopping time scales of 50 ps have been reported for monolayer and biolayer NC films,[17,62] while more recently, Cohen et al. have measured transfer time scales as fast as 30 ps in layered donor−acceptor NC structures treated with a short-chain dithiol that covalently links neighboring NCs.[15] Compared to these studies, the 200 fs exciton hopping time scale we obtain is roughly 2 orders of magnitude faster.

Given PDTC alters the spatial extent of photoexcited holes but not electrons,[32,33,52] it is not immediately clear why PDTC would speed exciton transfer over the transfer of holes between neighboring NCs. However, our data clearly show that exciton transfer dominates our observed dynamics. We observe rapid shifting of the B1 band of PDTC-functionalized NCs even though this band selectively reports on the behavior of photoexcited electrons over photoexcited holes,[57] suggesting the hole and electron move together. This notion is further supported by the decay of spectral features within our TA data. As the B1 band relaxes, we observe a near complete loss of other TA spectral features, suggesting B1 band relaxation occurs due to electron−hole recombination and not carrier trapping. Such recombination necessitates correlated motion of the photoexcited electron and hole.

One potential mechanism that could explain PDTC's large impact on exciton migration was recently outlined theoretically by Reich and Shklovskii,[63] who suggested exciton migration between NCs can occur via sequential hole- and electron-transfer steps. As the transfer of each charge carrier can occur in a concerted fashion, the formation of a charge-transfer intermediate is not necessitated but the rate of the overall exciton transfer depends on the strength of the one electron couplings for both electron and hole transfer. As such, increasing hole wave function overlap between NCs via PDTC functionalization would be expected to enhance exciton transfer via this mechanism. We note the exciton hopping rate we obtain agrees well with sub-picosecond time scales that have been reported for hole extraction from PDTC-functionalized nanomaterials,[35,38] suggesting that the rate of hole transfer limits exciton migration. Such a scenario would be expected for a concerted charge-transfer mechanism due to the hole's larger reduced mass.

Throughout this report, we have hypothesized that, due to the strong interaction of PDTC with NC valence band states,[32,33,39] PDTC promotes carrier wave function delocalization that improves electronic coupling between NCs that aids exciton transport. However, an alternate explanation for the improvement of exciton transport in NC films upon PDTC treatment is that PDTC ligands decompose within several hours after ligand exchange,[37] leaving behind a CdS shell on the NC surface that can direct oriented attachment between neighboring particles. Grenland et al. have used Raman spectroscopy to show that when PDTC ligands decompose, they deposit a thin shell of sulfur atoms that can bind strongly to a Cd^{2+}-enriched surface of a NC. They go on to propose this CdS shell is primarily responsible for carrier delocalization in this system.[64]

Despite these reports, a series of control experiments performed on PDTC films allow us to rule out PDTC decomposition as the origin of the rapid exciton transport we observe. First, FTIR measurements we have reported previously for PDTC-treated films[36] show PDTC ligands remain intact following the film-preparation and ligand-exchange procedures we employ. Next, scanning transmission electron microscopy (STEM) images of PDTC-treated NCs show they display an average interparticle distance greater than the expected separation for NCs that have fused epitaxially via a CdS shell (Figure S2). PDTC decomposition via laser-induced heating is also unlikely given that we need to heat PDTC-treated NC films to temperatures of 400−450 K to observe spectral changes attributed to particle necking,[54] such as the loss of a well-defined X1 band (Figure S9). This finding is consistent with prior studies that have employed dithiocarbamates as sulfur precursors for core−shell NC growth, which find these molecules need to be heated to temperatures above 410 K to produce appreciable shell growth.[65] We estimate the maximal temperature change imparted by absorption of our pump beam falls well below this threshold (section SVII of the Supporting Information). Finally, based on the estimated number of PDTC molecules per NC in our films obtained from FTIR and absorption spectra, a CdS shell deposited by PDTC decomposition would only partially coat the surface of a NC due to incomplete exchange of PDTC for oleate ligands. We would anticipate such a partial shell would lead to increased exciton trapping rather than enhancing the rate of exciton transport within the film. We note PDTC decomposition to aniline is catalyzed by acidic conditions.[66] Because PDTC is commonly synthesized as an ammonium salt, this makes PDTC decomposition sensitive to both the concentration of PDTC

DOI: 10.1021/acs.nanolett.8b01079
Nano Lett. XXXX, XXX, XXX−XXX

used and the length of the exchange process due to ammonia outgassing. Indeed, when PDTC-functionalized NCs have been removed from acidic conditions, they have been shown to be stable for upward of 62 h.[55] Under the conditions we use for solid-state ligand exchange, which limits the exposure of NC films to PDTC solutions to only 4 h, we find PDTC decomposition does not play a major role in our observations. This guides us to the conclusion that improved wave function overlap facilitated by PDTC ligand exchange leads to the rapid energy migration we report.

Conclusions. In summary, we have measured carrier transport dynamics in CdSe NC solids treated with an exciton-delocalizing ligand using a combination of fs-TA and kinetic Monte Carlo simulations. We have shown that solid-state ligand exchange with PDTC greatly improves transport properties in these films, as evidenced by a rapid decrease in the energy of photoexcited excitons on a sub-picosecond time scale. Modeling of these dynamics using KMC simulations reveals that PDTC increases the exciton hopping time scale to a value as fast as 200 fs, which stands among the fastest rates reported for exciton transfer between neighboring NCs. These simulations also highlight that preferential non-equilibrium relaxation at NCs with high degrees of PDTC substitution results in unique dynamics that reflect a competition between exciton transport and recombination pathways. While charge-carrier recombination presently limits the distances over which excitations diffuse in PDTC-substituted films, our results highlight that the strategy of employing exciton-delocalizing ligands to enhance energy transport in NC films is valid. Further work investigating the influence of such ligands on energy and charge transport in NC arrays is warranted.

Methods. *CdSe Nanocrystal Synthesis.* CdSe NCs were synthesized using a modified literature method.[67] Briefly, 420 mg of cadmium(myristate)$_2$ and 20 mL of 90% technical grade 1-octadecene were added to a three-neck round-bottom flask, vacuumed for 1 h, then purged under N_2 gas. After 1 h of purging, the reaction was heated to 250 °C under positive N_2 flow while being stirred vigorously throughout (500 rpm). Once the solution had reached 250 °C, 5 mL of a 0.1 M Se suspension (24 mg selenium in 6 mL 1-octadecene) was rapidly injected into the reaction, nucleating NC growth. The reaction was maintained at 240 °C until the solution reached a color indicative of NCs of a desired size. At this point, 3 mL of 90% technical grade oleic acid was injected into the reaction mixture. The solution was then stirred for an additional 3 min at 240 °C before cooling to room temperature. To remove the supernatant, the resulting mixture was dispersed in ethanol and centrifuged at 3200 rpm for 10 min. This process was repeated until a NC pellet had formed. NCs were then washed using 1:1 (v/v) *n*-hexane/ethanol and centrifuged for 10 min at 3200 rpm to remove excess oleate ligands and unreacted cadmium precursor. The liquid phase was removed, and this process repeated until the NCs became difficult to disperse in the *n*-hexane phase. The resulting NCs were then dispersed in 1 mL of 1:1 (v/v) *n*-hexane/octane for film preparation (~50 mg/mL) or dichloromethane for solution characterization.

PDTC Synthesis. PDTC was synthesized via a modified literature procedure[39] by chilling 5 mL of aniline in 30 mL of 30 w/w% ammonium hydroxide to 0 °C, maintained via an external ice bath, while stirring vigorously under N_2 flow. To this solution, 5 mL of carbon disulfide was added dropwise over 15 min. Following the carbon disulfide addition, the solution was stirred for 45 min at 0 °C before returning to room temperature. The resulting yellow-white precipitate was subsequently isolated via vacuum filtration, washed with dichloromethane, and stored in a desiccator in the dark. The final product was a fine white powder.

Nanocrystal Film Preparation. Prior to deposition of nanocrystal films, SiO_2 substrates were cleaned via sonication in chloroform, isopropyl alcohol, acetone, and toluene for 20 min each in that order. Following sonication, the substrates were stored in toluene until used for film deposition. Prior to spin-casting, the films were removed from the toluene bath and dried under N_2 flow. To produce the CdSe−oleate films used in this study, 60 μL of a ~50 mg/mL solution of nanocrystals in 1:1 (v/v) *n*-hexane/octane were dropped onto a spinning SiO_2 substrate. The spin-coating procedure used consists of spinning the substrate at 1000 rpm for 1 min, followed by an increase in the spin rate to 4000 rpm for an additional 10 s. This procedure produced optically clear, homogeneous films over a 1 in. × 1 in. square area (Figure 1). Temperature-dependent experiments were carried out using a Janis ST-100 cryostat, which was evacuated for 30 min prior to use. Temperatures were maintained throughout data collection using an external proportional-integral-derivative controller and liquid N_2 dispenser.

PDTC Ligand Exchange. Ligand exchange for PDTC was carried out by submerging as-cast CdSe−oleate films in a 10 mM PDTC solution in methanol (46.7 mg PDTC/25 mL methanol). During ligand exchange, films were kept in the dark and allowed to exchange for up to 4 h because this period was found to lead to a saturation of the observed red shift while yielding films with a high degree of optical transparency. Ligand exchanges that extended beyond this 4 h time window showed a marked decrease in the optical quality of the film.

Steady-State Optical Spectroscopy. Transmission and reflectance spectra were collected on a Shimadzu UV-2600 spectrophotometer with an ISR-2600 integrating sphere attachment. Both transmission and reflectance spectra were collected to properly account for reflective losses from the front face of sample films and used to calculate their absorption spectra. Emission spectra were collected on a Horiba Fluorolog3 spectrofluorimeter over a range of 2.58−1.55 eV using an integration time of 2 s. Spectra were collected in a right-angle collection geometry, in which the film was tilted 30° from normal to the excitation source. Films were excited using an excitation energy of 3.08 eV. Excitation and emission slit widths were set to yield a 2 nm spectral resolution.

Profilometry Measurements. Profilometry measurements were collected on a KLA Tencor Alpha-Step D-500 stylus profilometer. Prior to these measurements, CdSe−oleate and CdSe−PDTC films described above were scribed down to a 1 cm × 1 cm square, and a small portion of the film was removed by a razor blade, creating a step edge that exposed the SiO_2 substrate below each film. The stylus was scanned 0.4 mm across the step edge at a scan speed of 0.01 mm/s with a stylus force of 1.0 mg.

Scanning Transmission Electron Microscopy. Samples for STEM were prepared by submerging a lacey carbon-coated 200 mesh copper grid (SPI Supplies) into a ~10 μM solution of oleate-capped NCs in hexane for 30 s. For images of the ligand-exchanged samples, the grid was then dipped into a 10 mM PDTC solution in methanol for an additional 30 s prior to imaging. Images were collected with a high-angle annular dark field detector on a JEOL 2010f transmission electron microscope with an accelerating voltage of 200 kV.

DOI: 10.1021/acs.nanolett.8b01079
Nano Lett. XXXX, XXX, XXX−XXX

Scanning Electron Microscopy. Samples for SEM were prepared using the same procedure described in the Nanocrystal Film Preparation section apart from the use of a conductive ITO substrate. Images were collected on a Hitachi S5500 SEM with an accelerating voltage of 5 kV.

Transient Absorption Spectroscopy. A detailed description of the setup employed for TA can be found elsewhere.[36] Briefly, a femtosecond Ti:sapphire regenerative amplifier (Coherent Legend Duo Elite, 3 kHz, 4.5 mJ) was used to generate ∼90 fs pulses centered at 1.54 eV with a bandwidth of 160 cm^{-1} (full width at half-maximum). A small portion of the amplifier output (∼1 μJ) was focused into a 3 mm thick, c-cut sapphire window to produce broadband probe pulses (1.59−2.76 eV) via self phase-modulation. Pump pulses (3.1 eV) were generated by frequency doubling the fundamental Ti:sapphire output using a Type-I β-barium borate crystal. The pump fluence was selected such that all samples displayed a linear scaling of the differential absorbance amplitude with changing fluence (Figure S5). A rotation mount (Thorlabs KPRM1E) was used to continuously rotate the film at a rate of 25 deg/s throughout data collection to prevent charging effects. For temperature-dependent TA experiments, the cryostat housing a NC film was linearly translated throughout data collection using a computer-controlled delay stage (Newport XMS50) to prevent sample charging. Frequency-dependent instrument response functions (IRFs) for each scan were obtained using a cleaned SiO_2 substrate. Collection of the frequency-dependent IRFs allowed for chirp correction of the supercontinuum probe pulse.

■ ASSOCIATED CONTENT

Supporting Information

The Supporting Information is available free of charge on the ACS Publications website at DOI: 10.1021/acs.nanolett.8b01079.

Additional details and figures on the profilometry measurements of NC film thickness; STEM images and distributions for center-to-center distance analysis; TA spectra and analysis of PDTC ligand-exchanged CdSe NCs in solution; exponential fits for the extraction of k′ prefactor in the Miller−Abrahams rate equation; variation of TA signals with excitation fluence; temperature-dependent film absorption spectra; bleach peak energy and recovery; discussion of PDTC degradation upon film heating; and an expanded description of kinetic Monte Carlo simulations. (PDF)

■ AUTHOR INFORMATION

Corresponding Author

*E-mail: roberts@cm.utexas.edu.

ORCID

Adam P. Willard: 0000-0002-0934-4737

Sean T. Roberts: 0000-0002-3322-3687

Notes

The authors declare no competing financial interest.

■ ACKNOWLEDGMENTS

Work performed at UT Austin was supported by the National Science Foundation under award no. CHE-1610412, and work at MIT was supported by the Center for Excitonics, an Energy Frontier Research Center funded by the U.S. Department of Energy Office of Science and the Office of Basic Energy Sciences under award no. DE-SC0001088. M.S.A. acknowledges partial tuition support from a Hamilton/Schoch fellowship, and D.Y.Z. acknowledges support from an Undergraduate Research Fellowship provided by the Office of the Vice President for Research at the University of Texas at Austin. A.D. acknowledges support from the Natural Science and Engineering Research Council of Canada Postgraduate Scholarship Doctoral (NSERC PGS D) program. The authors also acknowledge the Texas Materials Institute at the University of Texas at Austin, which made available instrumentation for the characterization of NC films.

■ REFERENCES

(1) Talapin, D. V.; Lee, J.-S.; Kovalenko, M. V.; Shevchenko, E. V. Prospects of Colloidal Nanocrystals for Electronic and Optoelectronic Applications. *Chem. Rev.* **2010**, *110* (1), 389−458.

(2) Kagan, C. R.; Lifshitz, E.; Sargent, E. H.; Talapin, D. V. Building Devices from Colloidal Quantum Dots. *Science* **2016**, *353* (6302), aac5523.

(3) Chistyakov, A. A.; Zvaigzne, M. A.; Nikitenko, V. R.; Tameev, A. R.; Martynov, I. L.; Prezhdo, O. V. Optoelectronic Properties of Semiconductor Quantum Dot Solids for Photovoltaic Applications. *J. Phys. Chem. Lett.* **2017**, *8* (17), 4129−4139.

(4) Ginger, D. S.; Greenham, N. C. Charge Injection and Transport in Films of CdSe Nanocrystals. *J. Appl. Phys.* **2000**, *87* (3), 1361−1368.

(5) Liu, Y.; Gibbs, M.; Puthussery, J.; Gaik, S.; Ihly, R.; Hillhouse, H. W.; Law, M. Dependence of Carrier Mobility on Nanocrystal Size and Ligand Length in PbSe Nanocrystal Solids. *Nano Lett.* **2010**, *10* (5), 1960−1969.

(6) Yu, D.; Wang, C.; Guyot-Sionnest, P. n-Type Conducting CdSe Nanocrystal Solids. *Science* **2003**, *300*, 1277−1280.

(7) Guyot-Sionnest, P. Electrical Transport in Colloidal Quantum Dot Films. *J. Phys. Chem. Lett.* **2012**, *3* (9), 1169−1175.

(8) Yu, D.; Wehrenberg, B. L.; Jha, P.; Ma, J.; Guyot-Sionnest, P. Electronic Transport of n-Type CdSe Quantum Dot Films: Effect of Film Treatment. *J. Appl. Phys.* **2006**, *99* (10), 104315.

(9) Zarghami, M. H.; Liu, Y.; Gibbs, M.; Gebremichael, E.; Webster, C.; Law, M. p-Type PbSe and PbS Quantum Dot Solids Prepared with Short-Chain Acids and Diacids. *ACS Nano* **2010**, *4* (4), 2475−2485.

(10) Luther, J. M.; Beard, M. C.; Song, Q.; Law, M.; Ellingson, R. J.; Nozik, A. J. Multiple Exciton Generation in Films of Electronically Coupled PbSe Quantum Dots. *Nano Lett.* **2007**, *7* (6), 1779−1784.

(11) Carey, G. H.; Yuan, M.; Comin, R.; Voznyy, O.; Sargent, E. H. Cleavable Ligands Enable Uniform Close Packing in Colloidal Quantum Dot Solids. *ACS Appl. Mater. Interfaces* **2015**, *7* (39), 21995−22000.

(12) Ning, Z.; Ren, Y.; Hoogland, S.; Voznyy, O.; Levina, L.; Stadler, P.; Lan, X.; Zhitomirsky, D.; Sargent, E. H. All-Inorganic Colloidal Quantum Dot Photovoltaics Employing Solution-Phase Halide Passivation. *Adv. Mater.* **2012**, *24* (47), 6295−6299.

(13) Fan, J. Z.; Liu, M.; Voznyy, O.; Sun, B.; Levina, L.; Quintero-Bermudez, R.; Liu, M.; Ouellette, O.; García de Arquer, F. P.; Hoogland, S.; et al. Halide Re-Shelled Quantum Dot Inks for Infrared Photovoltaics. *ACS Appl. Mater. Interfaces* **2017**, *9* (43), 37536−37541.

(14) Gilmore, R. H.; Lee, E. M. Y.; Weidman, M. C.; Willard, A. P.; Tisdale, W. A. Charge Carrier Hopping Dynamics in Homogeneously Broadened PbS Quantum Dot Solids. *Nano Lett.* **2017**, *17* (2), 893−901.

(15) Cohen, E.; Komm, P.; Rosenthal-Strauss, N.; Dehnel, J.; Lifshitz, E.; Yochelis, S.; Levine, R. D.; Remacle, F.; Fresch, B.; Marcus, G.; et al. Fast Energy Transfer in CdSe Quantum Dot Layered Structures: Controlling Coupling with Covalent-Bond Organic Linkers. *J. Phys. Chem. C* **2018**, *122* (10), 5753−5758.

(16) Kholmicheva, N.; Moroz, P.; Eckard, H.; Jensen, G.; Zamkov, M. Energy Transfer in Quantum Dot Solids. *ACS Energy Lett.* **2017**, *2* (1), 154−160.

DOI: 10.1021/acs.nanolett.8b01079
Nano Lett. XXXX, XXX, XXX−XXX

(17) Achermann, M.; Petruska, M. A.; Crooker, S. A.; Klimov, V. I. Picosecond Energy Transfer in Quantum Dot Langmuir−Blodgett Nanoassemblies. *J. Phys. Chem. B* **2003**, *107* (50), 13782−13787.
(18) Koleilat, G. I.; Levina, L.; Shukla, H.; Myrskog, S. H.; Hinds, S.; Pattantyus-Abraham, A. G.; Sargent, E. H. Efficient, Stable Infrared Photovoltaics Based on Solution-Cast Colloidal Quantum Dots. *ACS Nano* **2008**, *2* (5), 833−840.
(19) Amin, V. A.; Aruda, K. O.; Lau, B.; Rasmussen, A. M.; Edme, K.; Weiss, E. A. Dependence of the Band Gap of CdSe Quantum Dots on the Surface Coverage and Binding Mode of an Exciton-Delocalizing Ligand, Methylthiophenolate. *J. Phys. Chem. C* **2015**, *119* (33), 19423−19429.
(20) Jang, J.; Dolzhnikov, D. S.; Liu, W.; Nam, S.; Shim, M.; Talapin, D. V. Solution-Processed Transistors Using Colloidal Nanocrystals with Composition-Matched Molecular "Solders": Approaching Single Crystal Mobility. *Nano Lett.* **2015**, *15* (10), 6309−6317.
(21) Kodaimati, M. S.; Wang, C.; Chapman, C.; Schatz, G. C.; Weiss, E. A. Distance-Dependence of Interparticle Energy Transfer in the Near-Infrared within Electrostatic Assemblies of PbS Quantum Dots. *ACS Nano* **2017**, *11* (5), 5041−5050.
(22) Wang, C.; Weiss, E. A. Sub-Nanosecond Resonance Energy Transfer in the Near-Infrared within Self-Assembled Conjugates of PbS Quantum Dots and Cyanine Dye J-Aggregates. *J. Am. Chem. Soc.* **2016**, *138* (30), 9557−9564.
(23) Lee, K.-R.; Bettis Homan, S.; Kodaimati, M.; Schatz, G. C.; Weiss, E. A. Near-Quantitative Yield for Transfer of Near-Infrared Excitons within Solution-Phase Assemblies of PbS Quantum Dots. *J. Phys. Chem. C* **2016**, *120* (39), 22186−22194.
(24) Beloborodov, I. S.; Lopatin, A. V.; Vinokur, V. M.; Efetov, K. B. Granular Electronic Systems. *Rev. Mod. Phys.* **2007**, *79* (2), 469−518.
(25) Abrahams, E.; Anderson, P. W.; Licciardello, D. C.; Ramakrishnan, T. V. Scaling Theory of Localization: Absence of Quantum Diffusion in Two Dimensions. *Phys. Rev. Lett.* **1979**, *42* (10), 673−676.
(26) Whitham, K.; Yang, J.; Savitzky, B. H.; Kourkoutis, L. F.; Wise, F.; Hanrath, T. Charge Transport and Localization in Atomically Coherent Quantum Dot Solids. *Nat. Mater.* **2016**, *15* (5), 557−563.
(27) Talgorn, E.; Gao, Y.; Aerts, M.; Kunneman, L. T.; Schins, J. M.; Savenije, T. J.; van Huis, M. A.; van der Zant, H. S. J.; Houtepen, A. J.; Siebbeles, L. D. A. Unity Quantum Yield of Photogenerated Charges and Band-like Transport in Quantum-Dot Solids. *Nat. Nanotechnol.* **2011**, *6* (11), 733−739.
(28) Kagan, C. R.; Murray, C. B. Charge Transport in Strongly Coupled Quantum Dot Solids. *Nat. Nanotechnol.* **2015**, *10* (12), 1013−1026.
(29) Choi, J.-H.; Fafarman, A. T.; Oh, S. J.; Ko, D.-K.; Kim, D. K.; Diroll, B. T.; Muramoto, S.; Gillen, J. G.; Murray, C. B.; Kagan, C. R. Bandlike Transport in Strongly Coupled and Doped Quantum Dot Solids: A Route to High-Performance Thin-Film Electronics. *Nano Lett.* **2012**, *12* (5), 2631−2638.
(30) Dong, A.; Jiao, Y.; Milliron, D. J. Electronically Coupled Nanocrystal Superlattice Films by in Situ Ligand Exchange at the Liquid−Air Interface. *ACS Nano* **2013**, *7* (12), 10978−10984.
(31) Crisp, R. W.; Callahan, R.; Reid, O. G.; Dolzhnikov, D. S.; Talapin, D. V.; Rumbles, G.; Luther, J. M.; Kopidakis, N. Photoconductivity of CdTe Nanocrystal-Based Thin Films: Te2− Ligands Lead To Charge Carrier Diffusion Lengths Over 2 μm. *J. Phys. Chem. Lett.* **2015**, *6* (23), 4815−4821.
(32) Frederick, M. T.; Weiss, E. A. Relaxation of Exciton Confinement in CdSe Quantum Dots by Modification with a Conjugated Dithiocarbamate Ligand. *ACS Nano* **2010**, *4* (6), 3195−3200.
(33) Frederick, M. T.; Amin, V. A.; Cass, L. C.; Weiss, E. A. A Molecule to Detect and Perturb the Confinement of Charge Carriers in Quantum Dots. *Nano Lett.* **2011**, *11* (12), 5455−5460.
(34) Jin, S.; Harris, R. D.; Lau, B.; Aruda, K. O.; Amin, V. A.; Weiss, E. A. Enhanced Rate of Radiative Decay in CdSe Quantum Dots upon Adsorption of an Exciton-Delocalizing Ligand. *Nano Lett.* **2014**, *14* (9), 5323−5328.
(35) Lian, S.; Weinberg, D. J.; Harris, R. D.; Kodaimati, M. S.; Weiss, E. A. Subpicosecond Photoinduced Hole Transfer from a CdS Quantum Dot to a Molecular Acceptor Bound Through an Exciton-Delocalizing Ligand. *ACS Nano* **2016**, *10* (6), 6372−6382.
(36) Azzaro, M. S.; Babin, M. C.; Stauffer, S. K.; Henkelman, G.; Roberts, S. T. Can Exciton-Delocalizing Ligands Facilitate Hot Hole Transfer from Semiconductor Nanocrystals? *J. Phys. Chem. C* **2016**, *120* (49), 28224−28234.
(37) Munro, A. M.; Chandler, C.; Garling, M.; Chai, D.; Popovich, V.; Lystrom, L.; Kilina, S. Phenyldithiocarbamate Ligands Decompose During Nanocrystal Ligand Exchange. *J. Phys. Chem. C* **2016**, *120* (51), 29455−29462.
(38) Lee, J. R.; Li, W.; Cowan, A. J.; Jäckel, F. Hydrophilic, Hole-Delocalizing Ligand Shell to Promote Charge Transfer from Colloidal CdSe Quantum Dots in Water. *J. Phys. Chem. C* **2017**, *121* (28), 15160−15168.
(39) Frederick, M. T.; Amin, V. A.; Swenson, N. K.; Ho, A. Y.; Weiss, E. A. Control of Exciton Confinement in Quantum Dot−Organic Complexes through Energetic Alignment of Interfacial Orbitals. *Nano Lett.* **2013**, *13* (1), 287−292.
(40) Nagpal, P.; Klimov, V. I. Role of Mid-Gap States in Charge Transport and Photoconductivity in Semiconductor Nanocrystal Films. *Nat. Commun.* **2011**, *2*, 486.
(41) Straus, D. B.; Goodwin, E. D.; Gaulding, E. A.; Muramoto, S.; Murray, C. B.; Kagan, C. R. Increased Carrier Mobility and Lifetime in CdSe Quantum Dot Thin Films through Surface Trap Passivation and Doping. *J. Phys. Chem. Lett.* **2015**, *6* (22), 4605−4609.
(42) Mora-Sero, I.; Bertoluzzi, L.; Gonzalez-Pedro, V.; Gimenez, S.; Fabregat-Santiago, F.; Kemp, K. W.; Sargent, E. H.; Bisquert, J. Selective Contacts Drive Charge Extraction in Quantum Dot Solids via Asymmetry in Carrier Transfer Kinetics. *Nat. Commun.* **2013**, *4*, 2272.
(43) Xu, J.; Voznyy, O.; Comin, R.; Gong, X.; Walters, G.; Liu, M.; Kanjanaboos, P.; Lan, X.; Sargent, E. H. Crosslinked Remote-Doped Hole-Extracting Contacts Enhance Stability under Accelerated Lifetime Testing in Perovskite Solar Cells. *Adv. Mater.* **2016**, *28* (14), 2807−2815.
(44) Chernomordik, B. D.; Marshall, A. R.; Pach, G. F.; Luther, J. M.; Beard, M. C. Quantum Dot Solar Cell Fabrication Protocols. *Chem. Mater.* **2017**, *29* (1), 189−198.
(45) Yang, Y.; Liu, Z.; Lian, T. Bulk Transport and Interfacial Transfer Dynamics of Photogenerated Carriers in CdSe Quantum Dot Solid Electrodes. *Nano Lett.* **2013**, *13* (8), 3678−3683.
(46) Gao, J.; Johnson, J. C. Charge Trapping in Bright and Dark States of Coupled PbS Quantum Dot Films. *ACS Nano* **2012**, *6* (4), 3292−3303.
(47) Kholmicheva, N.; Moroz, P.; Bastola, E.; Razgoniaeva, N.; Bocanegra, J.; Shaughnessy, M.; Porach, Z.; Khon, D.; Zamkov, M. Mapping the Exciton Diffusion in Semiconductor Nanocrystal Solids. *ACS Nano* **2015**, *9* (3), 2926−2937.
(48) Akselrod, G. M.; Prins, F.; Poulikakos, L. V.; Lee, E. M. Y.; Weidman, M. C.; Mork, A. J.; Willard, A. P.; Bulović, V.; Tisdale, W. A. Subdiffusive Exciton Transport in Quantum Dot Solids. *Nano Lett.* **2014**, *14* (6), 3556−3562.
(49) Lee, E. M. Y.; Tisdale, W. A. Determination of Exciton Diffusion Length by Transient Photoluminescence Quenching and Its Application to Quantum Dot Films. *J. Phys. Chem. C* **2015**, *119* (17), 9005−9015.
(50) Yoon, S. J.; Guo, Z.; dos Santos Claro, P. C.; Shevchenko, E. V.; Huang, L. Direct Imaging of Long-Range Exciton Transport in Quantum Dot Superlattices by Ultrafast Microscopy. *ACS Nano* **2016**, *10* (7), 7208−7215.
(51) Miller, A.; Abrahams, E. Impurity Conduction at Low Concentrations. *Phys. Rev.* **1960**, *120* (3), 745−755.
(52) Azpiroz, J. M.; De Angelis, F. Ligand Induced Spectral Changes in CdSe Quantum Dots. *ACS Appl. Mater. Interfaces* **2015**, *7* (35), 19736−19745.
(53) Alimoradi Jazi, M.; Janssen, V. A. E. C.; Evers, W. H.; Tadjine, A.; Delerue, C.; Siebbeles, L. D. A.; van der Zant, H. S. J.; Houtepen, A. J.; Vanmaekelbergh, D. Transport Properties of a Two-Dimensional

DOI: 10.1021/acs.nanolett.8b01079
Nano Lett. XXXX, XXX, XXX−XXX

PbSe Square Superstructure in an Electrolyte-Gated Transistor. *Nano Lett.* **2017**, *17* (9), 5238−5243.
(54) Webber, D. H.; Brutchey, R. L. Ligand Exchange on Colloidal CdSe Nanocrystals Using Thermally Labile Tert-Butylthiol for Improved Photocurrent in Nanocrystal Films. *J. Am. Chem. Soc.* **2012**, *134* (2), 1085−1092.
(55) Harris, R. D.; Amin, V. A.; Lau, B.; Weiss, E. A. Role of Interligand Coupling in Determining the Interfacial Electronic Structure of Colloidal CdS Quantum Dots. *ACS Nano* **2016**, *10* (1), 1395−1403.
(56) Klimov, V.; Hunsche, S.; Kurz, H. Biexciton Effects in Femtosecond Nonlinear Transmission of Semiconductor Quantum Dots. *Phys. Rev. B: Condens. Matter Mater. Phys.* **1994**, *50* (11), 8110−8113.
(57) Klimov, V. I.; McBranch, D. W. Femtosecond 1P-to-1S Electron Relaxation in Strongly Confined Semiconductor Nanocrystals. *Phys. Rev. Lett.* **1998**, *80* (18), 4028−4031.
(58) Schnitzenbaumer, K. J.; Labrador, T.; Dukovic, G. Impact of Chalcogenide Ligands on Excited State Dynamics in CdSe Quantum Dots. *J. Phys. Chem. C* **2015**, *119* (23), 13314−13324.
(59) Cui, J.; Beyler, A. P.; Coropceanu, I.; Cleary, L.; Avila, T. R.; Chen, Y.; Cordero, J. M.; Heathcote, S. L.; Harris, D. K.; Chen, O.; et al. Evolution of the Single-Nanocrystal Photoluminescence Linewidth with Size and Shell: Implications for Exciton−Phonon Coupling and the Optimization of Spectral Linewidths. *Nano Lett.* **2016**, *16* (1), 289−296.
(60) Gellen, T. A.; Lem, J.; Turner, D. B. Probing Homogeneous Line Broadening in CdSe Nanocrystals Using Multidimensional Electronic Spectroscopy. *Nano Lett.* **2017**, *17* (5), 2809−2815.
(61) Freyria, F. S.; Cordero, J. M.; Caram, J. R.; Doria, S.; Dodin, A.; Chen, Y.; Willard, A. P.; Bawendi, M. G. Near-Infrared Quantum Dot Emission Enhanced by Stabilized Self-Assembled J-Aggregate Antennas. *Nano Lett.* **2017**, *17* (12), 7665−7674.
(62) Franzl, T.; Shavel, A.; Rogach, A. L.; Gaponik, N.; Klar, T. A.; Eychmüller, A.; Feldmann, J. High-Rate Unidirectional Energy Transfer in Directly Assembled CdTe Nanocrystal Bilayers. *Small* **2005**, *1* (4), 392−395.
(63) Reich, K. V.; Shklovskii, B. I. Exciton Transfer in Array of Epitaxially Connected Nanocrystals. *ACS Nano* **2016**, *10* (11), 10267−10274.
(64) Grenland, J. J.; Lin, C.; Gong, K.; Kelley, D. F.; Kelley, A. M. Resonance Raman Investigation of the Interaction between Aromatic Dithiocarbamate Ligands and CdSe Quantum Dots. *J. Phys. Chem. C* **2017**, *121* (12), 7056−7061.
(65) Nan, W.; Niu, Y.; Qin, H.; Cui, F.; Yang, Y.; Lai, R.; Lin, W.; Peng, X. Crystal Structure Control of Zinc-Blende CdSe/CdS Core/Shell Nanocrystals: Synthesis and Structure-Dependent Optical Properties. *J. Am. Chem. Soc.* **2012**, *134* (48), 19685−19693.
(66) Humeres, E.; Debacher, N. A.; Franco, J. D.; Lee, B. S.; Martendal, A. Mechanisms of Acid Decomposition of Dithiocarbamates. 3. Aryldithiocarbamates and the Torsional Effect. *J. Org. Chem.* **2002**, *67* (11), 3662−3667.
(67) Pu, C.; Zhou, J.; Lai, R.; Niu, Y.; Nan, W.; Peng, X. Highly Reactive, Flexible yet Green Se Precursor for Metal Selenide Nanocrystals: Se-Octadecene Suspension (Se-SUS). *Nano Res.* **2013**, *6* (9), 652−670.

DOI: 10.1021/acs.nanolett.8b01079
Nano Lett. XXXX, XXX, XXX−XXX